

# Optical properties of structurally-relaxed Si/SiO<sub>2</sub> superlattices: the role of bonding at interfaces.

Pierre Carrier,<sup>1</sup> Laurent J. Lewis,<sup>1,\*</sup> and M. W. C. Dharma-wardana<sup>2</sup>

<sup>1</sup>*Département de Physique et Groupe de Recherche en Physique  
et Technologie des Couches Minces (GCM), Université de Montréal,  
Case Postale 6128, Succursale Centre-Ville, Montréal, Québec, Canada H3C 3J7*

<sup>2</sup>*Institute for Microstructural Sciences, National Research Council, Ottawa, Canada K1A 0R6*  
(Dated: May 21, 2019)

We have constructed microscopic, structurally-relaxed atomistic models of Si/SiO<sub>2</sub> superlattices. The structural distortion and oxidation-state characteristics of the interface Si atoms are examined in detail. The role played by the interface Si suboxides in raising the band gap and producing dispersionless energy bands is established. The suboxide atoms are shown to generate an abrupt interface layer about 1.60 Å thick. Bandstructure and optical-absorption calculations at the Fermi Golden rule level are used to demonstrate that increasing confinement leads to (a) direct bandgaps (b) a blue shift in the spectrum, and (c) an enhancement of the absorption intensity in the threshold-energy region. Some aspects of this behaviour appear not only in the symmetry direction associated with the superlattice axis, but also in the orthogonal plane directions. We conclude that, in contrast to Si/Ge, Si/SiO<sub>2</sub> superlattices show clear optical enhancement and a shift of the optical spectrum into the region useful for many opto-electronic applications.

submitted to Physical Review B

PACS numbers: 78.66.Jg, 68.65.+g, 71.23.Cq

## I. INTRODUCTION

The initial interest in light-emitting Si-based nanostructures has lead to a number of important experiments establishing that Si/SiO<sub>2</sub> superlattices (SLs) show enhanced, blue-shifted luminescence.<sup>1,2,3,4,5,6</sup> While the luminescence pattern is more complex in these systems than in others, the blue shift was found to correlate with decreasing Si-layer thickness. This simple relation between the silicon-layer thickness and the luminescence peak is of great interest for applications such as Si-based light-emitting diodes (Si-LEDs). All reported SL energy peaks are in the lower part of the visible spectrum — the highest reported value being 2.3 eV (540 nm), i.e., green,<sup>1</sup> and the lowest 1.2 eV (1030 nm), in the near infrared.<sup>3</sup> These SLs are really multiple Si quantum wells (MQW), the silicon oxide layers playing the role of barriers. The thickness of the Si quantum wells,  $L_{\text{Si}}$ , is the critical parameter. A fixed  $L_{\text{Si}}$  would simply set the colour of the Si-LED, while MQWs with a range of  $L_{\text{Si}}$  would span a range of colours in the luminescence.

Other systems containing confined silicon structures (besides MQWs) are, e.g., porous Si<sup>7,8</sup> (consisting of quasi one-dimensional structures), silicon nanoclusters in SiO<sub>2</sub> matrices,<sup>9</sup> nanocrystals<sup>10</sup> or dislocation loops, and quantum-dot structures made from implantation of boron<sup>11</sup> or other ions.<sup>12</sup> The choice of a particular structure, e.g., for Si-LED applications, depends on many factors: stability over time, optical efficiency at room temperature, experimental reproducibility, facility to accept n- or p- type dopants (e.g., for n-p junctions), ease of incorporation in ultra-large-scale-integration technology, and production costs. Si/SiO<sub>2</sub> SLs are stable struc-

tures, as opposed to porous-Si. In addition, the silicon layer thicknesses in SLs are directly related to the energy peaks in the Si/SiO<sub>2</sub> luminescence spectra. This is not straightforward in porous silicon, Si clusters or nanocrystals, where pore dimensions as well as hydrogen concentrations play an uncontrolled role on the energy shift.<sup>13</sup>

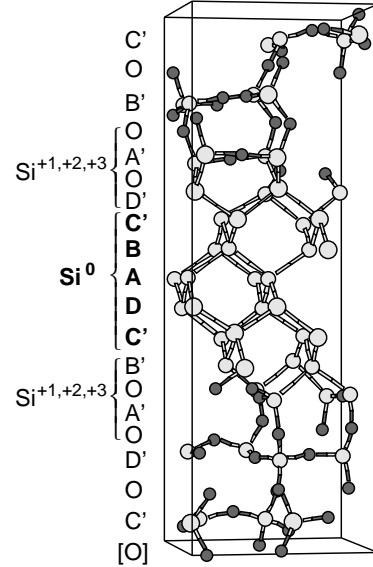


FIG. 1: The unit cell of the fully relaxed SL model (FRM1). The configuration of the bulk-like and suboxide Si atomic planes is also depicted. The white and black circles are respectively the positions of Si and O atoms.

Silicon-based structures have many advantages over structures made of other semiconductors: low-cost (as compared to any of the III-V's or II-VI's), non-toxicity, practically unlimited availability (in contrast to germanium) and benefits from decades of experience in purification, growth, and device fabrication. However, the indirect energy gap ( $\sim 1.1$  eV) in bulk crystalline silicon (c-Si) makes it unsuitable for optoelectronic applications. Silica ( $\text{SiO}_2$ ) is another key material of the microelectronics industry; it has a bandgap of  $\sim 9$  eV. Optical-fiber technologies and metal-oxide-semiconductor field-effect transistors (MOSFETs) are based on (high-quality) silica. Molecular-beam epitaxy and chemical vapor deposition provide the needed growth technology for Si and  $\text{SiO}_2$ . It is possible to combine crystalline silicon<sup>2,14,15</sup> and  $\text{SiO}_2$  to produce structured materials having chemically pure, sharp, defect-free interfaces. The degree of advancement of the fabrication technology is such that the enhanced luminescence in Si/ $\text{SiO}_2$  SLs *cannot* be explained in terms of defects, or residual hydrogen atoms filling Si dangling bonds at the SL interfaces, as in the well-understood luminescence of *a*-Si:H.

The objective of the present article is to consider the detailed microscopic structure of the  $\text{SiO}_2/\text{Si}/\text{SiO}_2$  double interface structure and provide a first-principles understanding of the emission of light from Si/ $\text{SiO}_2$  SLs. Only a few atomistic DFT calculations on Si/ $\text{SiO}_2$  SLs have been reported.<sup>16,17,18,19,20,21</sup> Many more would have been available were it not of the (naturally-occurring) amorphous structure of  $\text{SiO}_2$ : amorphous structures require large supercells to get physically relevant results. Another important issue is the need to model the Si/ $\text{SiO}_2$  interface so as to correctly incorporate the known experimental details. Recent core-level shift measurements<sup>22</sup> provide details of the suboxide (partially oxidized) Si atoms.<sup>23</sup> Further, the abruptness of the Si/ $\text{SiO}_2$  interface has been established from transmission electronic microscopy (TEM) experiments; values of the interface width as low as 5 Å have been reported.<sup>2,24</sup> Based on these observations, realistic Si/ $\text{SiO}_2$  interface models have been designed by several workers.<sup>25,26,27,28,29,30</sup> Suboxide Si atoms in most of these models are distributed within three atomic layers of the Si/ $\text{SiO}_2$  interface, corresponding to the lowest experimental interface thickness. Such interface models are needed for first-principles modelling of MOSFETs, and for SL structures, where *multiple* Si/ $\text{SiO}_2$  interfaces are present.

An early (and tractable) Si/ $\text{SiO}_2$  interface model was proposed by Herman and Batra.<sup>31</sup> The large lattice mismatch between  $\text{SiO}_2$  and Si was accommodated by setting the  $\beta$ -cristobalite  $\text{SiO}_2$  unit cell diagonally on the diamond-like c-Si unit cell. An oxygen atom was included in the interface to saturate the dangling bonds, resulting in a crystalline model of the interface. Another simple crystalline model, involving a bridge oxygen at the interface, was introduced by Tit and Dharma-wardana.<sup>32</sup> These models were studied using a variety of methods — tight-binding (TB),<sup>31,32</sup> full-potential, linear-muffin-

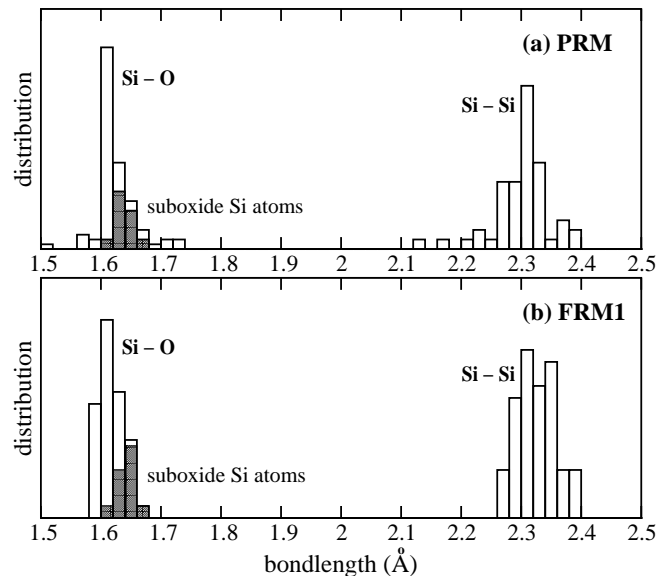


FIG. 2: Evolution of the Si-O and Si-Si bondlengths from (a) the PRM construction by Tit and Dharma-wardana, to (b) the fully relaxed structure (FRM1) described in the text.

tin-orbitals (FP-LMTO)<sup>18,19</sup> and linearized-augmented-plane-waves (FP-LAPW).<sup>20</sup> The dispersionless character of the bandstructure in the growth axis has been confirmed within all three theoretical approaches, thus demonstrating the existence of strong confinement. However, the nature of the energy gap — from both LMTO and LAPW calculations — is still indirect. Furthermore, these crystalline models show that the light absorption is quite dependent on the details of bonding and interface structure (bondlengths, angles and chemical species), emphasizing the need for *more realistic, structurally-relaxed* models.<sup>20</sup>

Several structurally-relaxed models have been investigated by Kageshima and Shiraishi using first-principles methods. Their models were constructed starting from  $\beta$ -cristobalite as well as  $\alpha$ -quartz  $\text{SiO}_2$  layers superposed onto c-Si layers with different possibilities for the Si/ $\text{SiO}_2$  interface (such as hydrogen atoms at dangling bonds);<sup>17</sup> the atomic sites were then structurally relaxed. The calculations indicate that the energy gaps are indeed direct, and that interfacial Si-OH bonds are possible candidates for the light-emitting enhancement in SLs. However, the models are not consistent with the observed suboxide Si atomic distributions at the Si(001)/ $\text{SiO}_2$  interfaces. For instance, no Si atoms bonded to three oxygens are present. Tit and Dharma-wardana<sup>33</sup> have constructed a partially-relaxed model (PRM) starting from a structurally relaxed Si(001)/ $\text{SiO}_2$  interface structure due to Pasquarello, Hybertsen, and Car (PHC).<sup>25</sup> This interface model contains all three suboxide Si atomic species. Hydrogen atoms were used by PHC to terminate the surface. In the Tit and Dharma-wardana model, the H atoms were removed and the Si/ $\text{SiO}_2$  interface structure was converted into a  $\text{SiO}_2/\text{Si}/\text{SiO}_2$  double interface SL

structure while preserving local tetrahedral bonding to obtain the PRM structure. Within the TB approach, the energy gap of the PRM was shown to be direct and enhancement of the optical properties (as compared to c-Si) was confirmed.<sup>34</sup> This is further described in the next section, since the fully relaxed models (FRMs) discussed in the present work are based on this PRM.

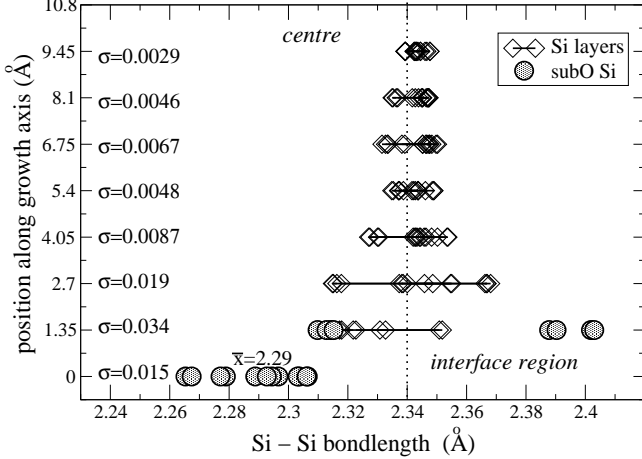


FIG. 3: Si-Si bondlength distribution in the FRM3, from the interface (bottom of figure) towards the center (top of figure) of the Si layer. (There are thirteen Si<sup>0</sup> layers in the FRM3 and thus six interplanar Si-Si bondlengths starting from both interfaces towards the center of the Si layer.

The results presented here go beyond the TB approach and were obtained within the projector-augmented wave (PAW) theoretical framework. A brief description of the theory is given in section II. The SL models were all structurally relaxed, and contain no hydrogen atoms at the interfaces. The interface suboxide Si atoms observed in experiment<sup>23</sup> arise naturally in the model. Calculations were carried out for different Si-layer thicknesses, in order to assess the effect of confinement on the electronic and optical properties. Supplementary models have been constructed to clarify the role of the suboxide atoms on the SL optical properties. We first review the theoretical methods (section II), then focus on the four central issues needed to understand the Si/SiO<sub>2</sub> luminescence properties: construction of realistic interface models (section III), quantum confinement (section IV), role of the suboxide atoms (section V), and optical effects associated with increased confinement (section VI). Our study thus provides a complete, microscopic picture of the luminescence properties of Si/SiO<sub>2</sub> SLs.

## II. COMPUTATIONAL DETAILS

The electronic-structure calculations were carried out using the Vienna *ab initio* simulation package (VASP)<sup>35</sup> using the “frozen-core” PAW approach.<sup>36</sup> The overall framework is density-functional theory<sup>37,38</sup> (DFT) within

the local-density approximation (LDA).<sup>39</sup>

The “frozen-core” PAW is a simpler form of the general PAW method introduced by Blöchl.<sup>40</sup> Blöchl’s method is an extension of the usual LAPW<sup>41</sup> approach. Hence, the PAW method formally bridges the LAPW to the ultrasoft-pseudopotentials (US-PP) in order to combine the precision of the former and the rapidity (for larger systems) of the latter. The PAW method has another advantage over the usual implementation of US-PP, essential for optical calculations: it avoids correcting for spatial nonlocality effects in typical pseudopotentials when evaluating the momentum operator  $\mathbf{p}$ . Further details can be found in the article of Adolph *et al.*<sup>42</sup>

Matrix elements of the momentum operator  $\mathbf{p}$  are needed for calculating interband optical effects. We describe the main steps that lead to the calculation of the absorption coefficient, starting from PAW solutions of the Kohn-Sham equations. The PAW approach rests on the following linear transformation:

$$|\Psi_N\rangle = |\tilde{\Psi}_N\rangle + \sum_i \left( |\phi_N\rangle - |\tilde{\phi}_N\rangle \right) \langle \tilde{p}_i | \tilde{\Psi}_N \rangle.$$

This relates the (calculated) pseudo wave function  $|\tilde{\Psi}_N\rangle$  to the (now corrected) all-electrons wave function  $|\Psi_N\rangle$ . The index specifies the atomic site, angular momentum numbers and reference energy. The two functions  $|\tilde{\phi}_N\rangle$  and  $|\phi_N\rangle$  are respectively the pseudo, and all-electron wave function of a reference atom. They are forced to overlap outside a given core region. The functions  $|\tilde{p}_i\rangle$  are the *projector* functions characteristic of the PAW method. Thus, the three functions  $|\phi_N\rangle$ ,  $|\tilde{\phi}_N\rangle$  and  $|\tilde{p}_i\rangle$  constitute the frozen-core PAW data, being set prior to self-consistent field calculations. The projector functions  $|\tilde{p}_i\rangle$  are constructed so as to remain dual to the pseudo wave functions, to fulfill generalized orthogonality constraints and to remain (approximately) complete (see Ref. 42 for full definitions).

The application of the above linear transformation to any operator  $A$  within the PAW approach has been described by Blöchl [cf. eq. (11) of Ref. 40]. If  $A$  is the momentum operator  $\mathbf{p}$  (in a certain direction defined by the polarization vector), we have

$$\langle \Psi_N | \mathbf{p} | \Psi_M \rangle = \langle \tilde{\Psi}_N | \mathbf{p} | \tilde{\Psi}_M \rangle + \sum_{i,j} \langle \tilde{\Psi}_N | \tilde{p}_i \rangle \left( \langle \phi_i | \mathbf{p} | \phi_j \rangle - \langle \tilde{\phi}_i | \mathbf{p} | \tilde{\phi}_j \rangle \right) \langle \tilde{p}_j | \tilde{\Psi}_M \rangle.$$

The imaginary part of the dielectric function,  $\epsilon_i$ , can be determined by using the Fermi Golden rule within the Coulomb gauge; the expression becomes:<sup>43</sup>

$$\epsilon_i(E) = \frac{\kappa^2}{E^2} \sum_{M,N} \int_{BZ} \frac{2d^3\vec{k}}{(2\pi)^3} |\langle \Psi_N | \mathbf{p} | \Psi_M \rangle|^2 \times f_N(1-f_M) \delta(E_N - E_M - E),$$

where  $\kappa = 2\pi e/m$ . The function  $f_n$  is the Fermi distribution and  $\langle \Psi_N | \mathbf{p} | \Psi_M \rangle$  are the PAW matrix elements. The

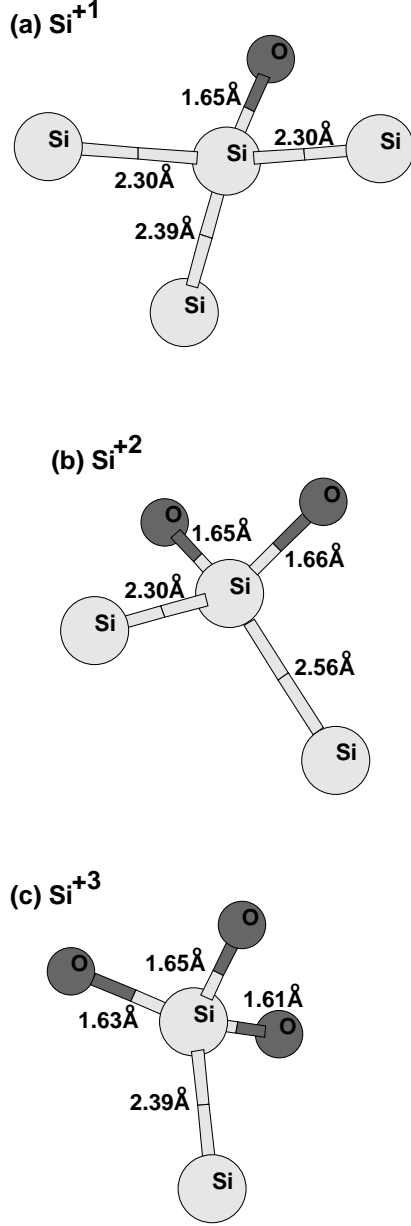


FIG. 4: Structure of the three suboxide interfacial Si atoms.

whole expression corresponds to the probability per unit volume for a transition of an electron from the valence band state  $|\Psi_N\rangle$  to the conduction band state  $|\Psi_M\rangle$  to occur.

The tetrahedron method<sup>44</sup> is used to evaluate  $\epsilon_i(E)$ . The joint density of states, which determines the interband transitions  $\delta(E_N - E_M - E)$  and the optical matrix elements  $|\langle\Psi_N|\mathbf{p}|\Psi_M\rangle|^2$ , are computed on each tetrahedron (i.e.,  $1/4 \times$  the sum of the matrix elements on the four corners of each tetrahedron). The real part  $\epsilon_r$  is then obtained using the Kramers-Kronig relation.<sup>43</sup> Since the dielectric function is the square of the complex refractive

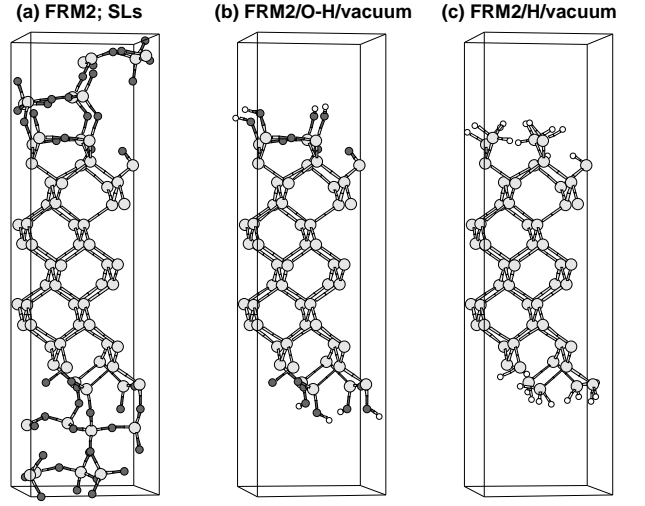


FIG. 5: (a) The FRM2 SLs (b) the FRM2/O-H/vacuum model (c) the FRM2/H/vacuum model.

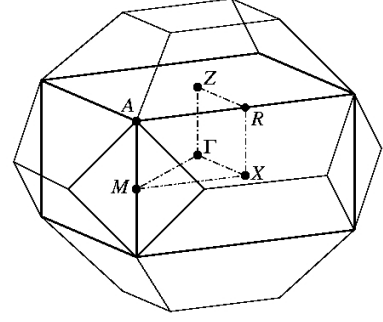


FIG. 6: Definition of the SLs BZ superposed to the diamond-like BZ. The principal axis used for bandstructure calculation are also depicted.

index,  $(\epsilon_r + i\epsilon_i) = (n_r + in_i)^2$ , the absorption coefficient becomes

$$\alpha(E) = 4\pi \frac{E}{hc} n_i = 4\pi \frac{E}{hc} \left[ \frac{(\epsilon_r^2 + \epsilon_i^2)^{1/2} - \epsilon_r}{2} \right]^{1/2}$$

with  $c$  the speed of light in vacuum,  $h$  Planck's constant, and  $E$  the photon energy.

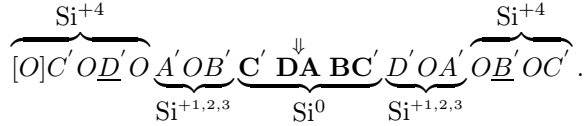
Electron-hole (e-h, excitonic) interactions were not included in the calculations, as they would be in, say, solutions of the Bethe-Salpeter equation. The size of our systems prohibits such complete optical calculations, which are feasible only for very small systems (a few atoms). These additional effects would enhance the results from interband transitions since e-h interactions generally increase the absorption at the onset.<sup>45</sup>

### III. CONSTRUCTION OF THE STRUCTURAL MODELS

Recent core-level shift experiments<sup>23</sup> have revealed the presence of all possible oxidation states for Si atoms in Si/SiO<sub>2</sub> structures such as SLs, that is Si<sup>+*n*</sup>, where *n* = 0, 1, 2, 3, 4 is the charge found within each Si Wigner-Seitz sphere. Si<sup>0</sup> and Si<sup>+4</sup> are the charge states of Si found in bulk-Si and bulk-SiO<sub>2</sub>. The suboxide (subO) Si atoms with *n* = 1, 2, 3 are found at the interface. Slightly larger distributions for the subO Si<sup>+3</sup> densities, as compared to those for Si<sup>+1</sup> and Si<sup>+2</sup>, were reported in these experiments. Microscopic Si/SiO<sub>2</sub> interface models should be consistent with experiments in closely reproducing the density distributions of *all* subO Si atoms.

As mentioned above, the Si/SiO<sub>2</sub> SL model structures discussed in the present article are based on the Si(001)/SiO<sub>2</sub> interface structures obtained by PHC,<sup>25</sup> who used the Car-Parrinello method to relax the models to their energy minimum. It is important to note that the PHC models were *not* designed for the double interface structure found in SiO<sub>2</sub>/Si/SiO<sub>2</sub> SLs but, rather, for a single Si/SiO<sub>2</sub> interface which terminates into the vacuum; this is done by saturating dangling bonds with H atoms. Thus, these models *de facto* contain the essential details of atomic positions and charge states at the Si/SiO<sub>2</sub> interface.

Tit and Dharma-wardana<sup>33</sup> have generated a Si/SiO<sub>2</sub> SL structure starting from one of the PHC models that contains an *equal* distribution of the three subO atoms, in (almost complete) accord with experiment. This SL model has been constructed by first operating a mirror transformation and then a partial rotation of the Si/SiO<sub>2</sub> section of the relaxed interface structure, leading to an intermediate Si/SiO<sub>2</sub>[mirror]SiO<sub>2</sub>/Si SL structure. Second, some of the Si layers were inverted in order to meet the *sp*<sup>3</sup>-bonding topology. The resulting Si/SiO<sub>2</sub> SLs structure, fully described in the article of Tit and Dharma-wardana,<sup>33</sup> has the following final configuration,



The connection between the symbols in this configuration and the specific atomic layers in the model is shown in Fig. 1. The letters *A*, *B*, *C* and *D* correspond to silicon atomic layers, while the *O*s are oxygen layers. The primes denote layers that depart from the diamond-like-Si crystalline arrangement, and [*O*] corresponds to the layer where the mirror operation has been performed.  $\underline{B'}$  and  $\underline{D'}$  are the Si layers which have been inverted in order to satisfy the *sp*<sup>3</sup>-bonding topology. The subO Si<sup>+*n*</sup> atoms, with *n* = 1, 2, 3, are distributed within only two Si layers, while the Si<sup>0</sup> atoms are distributed within five atomic layers. The embryonic PHC interface model corresponds roughly to one side of the above configuration, starting from the arrow up to the right.

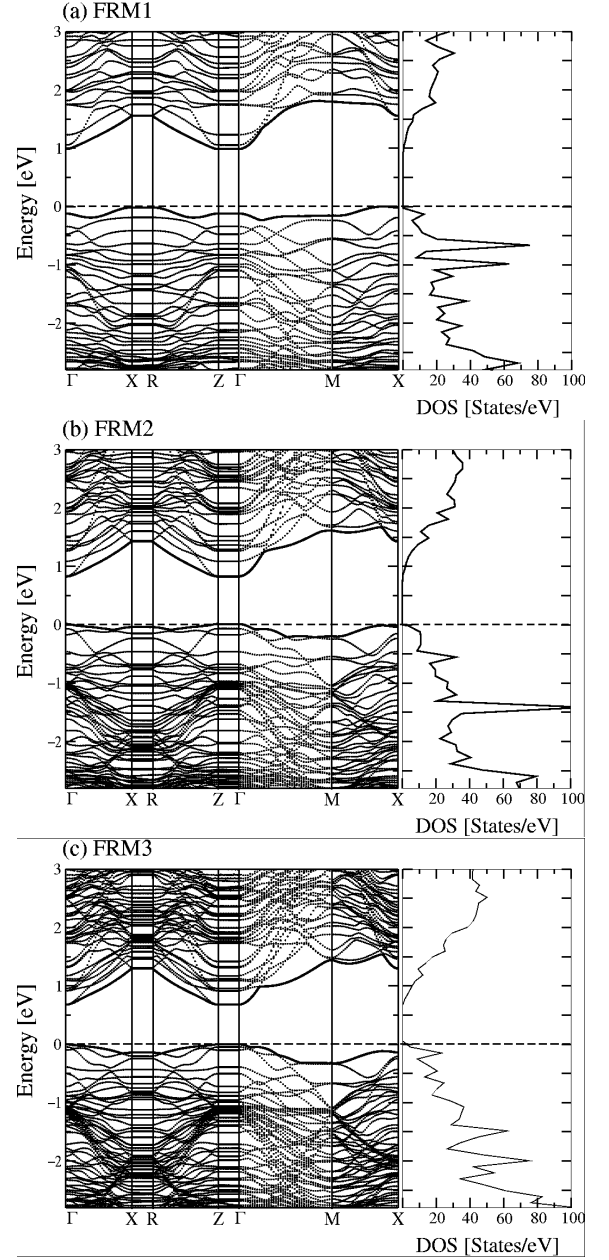


FIG. 7: Band structures and density of states (DOS) of the three SL models.

Of course, this construction induces artificial symmetries in the middle of the SiO<sub>2</sub> layer (more precisely, upon and around the [*O*] layer); this model is thus in essence *partially* relaxed — the PRM referred to earlier. Significant information on the electronic and optical properties of this model have been extracted, within the TB approach, by Tit and Dharma-wardana,<sup>33</sup> who obtained direct energy gaps as well as dispersionless bandstructures. Furthermore, the imaginary part of the dielectric function was calculated. The enhancement of the optical properties, and the blueshift with confinement, have been demonstrated by calculating the absorption coefficient.<sup>34</sup>

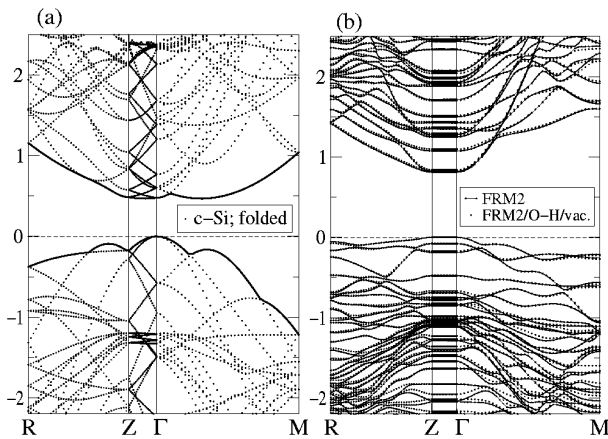


FIG. 8: Band structures of (a) c-Si in the (folded) SL BZ (b) comparison between the FRM2 SLs and the FRM2/O-H/vacuum bandstructures.

The next obvious step is to relax the PRM, i.e., determine the set of positions which leads, via the Hellman-Feynman forces, to the lowest total energy. We have used the PAW approach described in the previous section to obtain a first fully-relaxed model (FRM1), which contains approximately one unit cell of confined-Si. The supercell contains 52 Si and 44 O atoms, and has dimensions  $7.675 \times 7.675 \times 24.621 \text{ \AA}^3$ . Five  $\mathbf{k}$  points in the reduced Brillouin zone (BZ) were necessary to achieve the relaxation. The energy cutoff was 25.96 Ryd in all calculations. The total energy was found to decrease by 30.84 eV (0.32 eV per atom) during relaxation. Figure 2 shows the bondlength distributions before (PRM) and after (FRM1) relaxation; the bondlengths are centered around the expected values, viz.,  $\sim 1.61 \text{ \AA}$  for Si-O and  $2.35 \text{ \AA}$  for Si-Si bonds. The shaded boxes in Fig. 2 are the distributions of the interface subO Si atoms, while the empty boxes are the total distribution bondlengths, including subO Si atoms; the shaded boxes remain relatively unchanged upon relaxation since both interfaces were already at their energy minimum, after PHC. The main atomic drift during relaxation occurs mainly in the center of the Si and SiO<sub>2</sub> layers, i.e., near the [O] and the A layer of the configuration discussed above. Interfacial Si-O bondlengths of all subO Si atoms depart from the values of Si<sup>+4</sup> in the SiO<sub>2</sub> layer. The broadening of the Si-Si bondlengths is in general much larger than that of Si-O; the distortion of the bondlengths are thus mainly within the Si layer and at the Si/SiO<sub>2</sub> interface, i.e., not inside the silica layer. This is further discussed below. The resulting FRM1 is shown in Fig. 1.

Additional models having thicker Si wells were constructed in order to examine the role of subO Si layers and the effect of confinement on the electronic and optical properties. As noted earlier, the FRM1 structure contains approximately one unit cell of confined-Si, i.e., the set of layers with charge state Si<sup>0</sup> (bulk-like Si). By inserting one, then two, additional *ABCD* Si atomic planes

(i.e., one Si unit cell, thickness  $5.43 \text{ \AA}$ ), and relaxing all atoms, we generated two additional models – FRM2 and FRM3. The FRM2 contains 68 Si atoms while the FRM3 has 84 Si atoms; both have 44 oxygen atoms, as in the FRM1. The *total* energy variation for the FRM2 during relaxation was found to be only 0.15 eV (i.e., 0.0013 eV/atom) while for the FRM3, this change is a minuscule 0.051 eV (i.e., 0.00040 eV/atom). These numbers imply that both FRM2 and FRM3 have essentially crystalline Si layers. The FRM2 has nine Si<sup>0</sup> atomic planes while the FRM3 has thirteen.

Figure 3 shows the distributions of the Si-Si bondlengths in the FRM3, starting from the Si(001)/SiO<sub>2</sub> interfaces (at the bottom of Fig. 3) and going towards the centre of the silicon layer along the growth axis. The standard deviation ( $\sigma$ ) from the mean value ( $\bar{x}=2.34 \text{ \AA}$  in all atomic layers except at the interface, where  $\bar{x}=2.29 \text{ \AA}$ ) is also given. The diamond-shaped symbols correspond to the Si-Si bondlengths for Si<sup>0</sup> atoms while the filled circles are subO Si-Si bondlengths at the interfaces. The Si-Si bondlengths depart significantly from their crystalline counterparts at the interfaces up to about three atomic layers, where  $\sigma=0.019$ ; the standard deviation is four times higher at the interfaces than in the fifth atomic layer. This deviation of the bondlengths at the Si/SiO<sub>2</sub> interfaces shows that it is important to take relaxation aspects into account. This is further discussed in section V.

The three subO Si configurations at the interfaces of the FRMs are shown in Fig. 4 with their corresponding bondlengths. Note that the left and right interfaces in the SiO<sub>2</sub>/Si/SiO<sub>2</sub> SLs are not *exactly* equivalent; they remain independent (during structural relaxation, for instance). However, a subO Si on the left interface has a locally equivalent subO Si on the right interface, by construction. As a consequence, each pair of equivalent subO Si atoms have approximately the same bondlengths and angles in all the FRMs. As seen in Fig. 4, the bondlengths depart from their bulk values, which are  $2.35 \text{ \AA}$  for c-Si and  $1.61 \text{ \AA}$  for SiO<sub>2</sub>. In addition, the angles of the subO Si tetrahedra vary considerably: the Si-Si-Si angles vary from  $99^\circ$  to  $125^\circ$ , the O-Si-Si angles vary from  $96^\circ$  to  $126^\circ$ , while all O-Si-O angles remain around  $106^\circ$ . It is thus clear that the subO Si tetrahedra at the interfaces are distorted as compared to bulk-Si tetrahedra.

As discussed later on, the role of subO Si atoms was further studied using the following variations of the FRM2: First, we removed all Si<sup>+4</sup> atoms and attached the proper number of hydrogen atoms to neutralize the excess charges. The H positions were then relaxed while keeping all the silicon and oxygen atoms fixed. This structure thus contains Si<sup>0</sup> atoms and Si<sup>+n</sup> subOs, where  $n = 1, 2, 3$  (i.e.,  $n \neq 4$ ). A variation of this structure was generated by removing all oxygen atoms and filling the Si dangling bonds with H atoms, and again relaxing the H atoms. The final Si-H bondlengths vary from  $1.47 \text{ \AA}$  to  $1.53 \text{ \AA}$ , after relaxation. This final structure is thus subO-free and contains only Si<sup>0</sup> atoms, except at

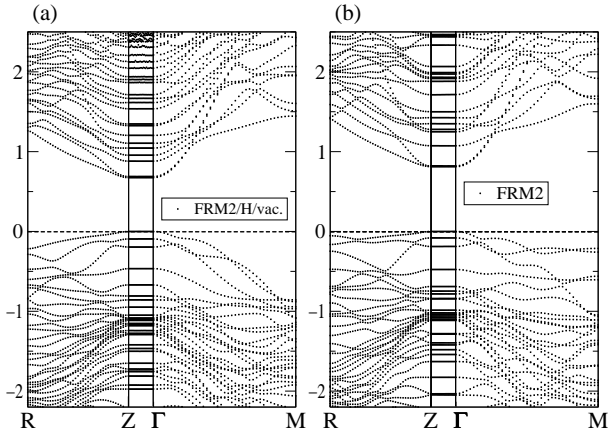


FIG. 9: Comparison of the bandstructures for (a) FRM2/H/vacuum and (b) FRM2 SLs.

the interface with the vacuum, where hydrogen atoms fill the dangling bonds. These three confinement models are shown in Fig. 5; they will be referred to as “FRM2”, “FRM2/O-H/vacuum” and “FRM2/H/vacuum”, respectively.

In Fig. 6 we show the BZ of the supercell, the standard c-Si diamond BZ, and the high symmetry axes used for the bandstructure calculations. We also constructed the bulk c-Si structure in a supercell of dimensions similar to that of the FRM SLs, so that comparisons can be done within the same  $\mathbf{k}$  space zone scheme. This will be used in the next three sections for comparisons of bandstructure as well as absorption calculations.

#### IV. QUANTUM CONFINEMENT

In this section, we discuss the nature of the confined states in the SLs. We calculated the bandstructures of the three SL models — FRM1, FRM2 and FRM3 — as well as the supplementary FRM2/O-H/vacuum structure, cf. Fig. 5(b). The latter is the “ultimate” in terms of confinement, as the two interfaces with vacuum constitute infinite potential walls. All bandstructures are analysed and compared within equivalent supercell BZ. The growth axis of the SLs being the  $z$ -axis, confinement effects are expected to take place in the  $X$ - $R$  and  $Z$ - $\Gamma$  axis of the BZ (see Fig. 6 for axis definitions).

The bandstructures of the three SLs and their total density of states (DOS) are shown in Fig. 7. We find that the bandstructures in the growth axis ( $X$ - $R$  and  $Z$ - $\Gamma$ ) are dispersionless, for all models and all energies. In physical terms, dispersionless bandstructures imply infinite effective masses, reflecting the strong confinement. The DOS have a more abrupt variation in the valence bands than in the conduction bands. However, DOS alone are not enough to fully understand the optical processes involving the interband transitions, since the weighting of the optical matrix elements is needed. This is further

discussed in Section VI.

Let us consider in more details one of the SL models, namely the FRM2. We select the  $R$ - $Z$ - $\Gamma$ - $M$  high-symmetry axis where the major features, viz. the relevant energy gaps, appear. The bandstructures of the folded c-Si structure, the FRM2 SLs structure as well as the FRM2/O-H/vacuum structure have been calculated and compared. Figure 8(a) and 8(b) contain a synopsis of all calculations for  $\mathbf{k}$  points along  $R$ - $Z$ - $\Gamma$ - $M$ . Several conclusions can be drawn from these figures.

By comparing the bands for c-Si, Fig. 8(a), with those for the FRM2 SL, Fig. 8(b) (solid lines), we see that folding effects cannot by themselves explain the new bandstructure. The bands in the  $Z$ - $\Gamma$  directions are totally modified by the confinement. The bandgap of c-Si in its folded configuration is nearly direct, while for the SL the bandgap is *unequivocally* direct, and significantly increased. Moreover, comparing the bands in a direction orthogonal to the growth axis, for instance around  $M$  in both Fig. 8(a) and Fig. 8(b), we see that the valence bands are raised; the lowest conduction band in the  $\Gamma$ - $M$  direction is pushed to higher energies. In addition, they exhibit less dispersion in the SL than in c-Si, in general. Hence, confinement modifies the electronic properties in the growth axis as well as in directions orthogonal to it. This is further analysed from optical absorption calculations, below.

We compare in Fig. 8(b) the bandstructures of the FRM2 and FRM2/O-H/vacuum models. The positions of the  $\text{Si}^0$  atoms, as well as the subO Si in the two structures, are identical. The solid lines displays the bandstructures of the FRM2, while the dots display the bands of the FRM2/O-H/vacuum structure. It is clear that the two bandstructures are nearly identical. This calculation shows that the  $\text{SiO}_2$  layers act as virtually impenetrable barriers. The electronic properties of hypothetical SL structures having only subO Si — i.e., no  $\text{Si}^{+4}$  of  $\text{SiO}_2$  — and positioned at the subO Si sites, would give nearly identical electronic properties as Si/ $\text{SiO}_2$  SLs, for energies close to the band gap. Our calculations show that the electronic wavefunctions die out at the suboxide Si atoms of the interfaces. Thus the barrier is sharply located just behind the subO Si atoms, and therefore just two atomic layers could be used as a barrier without altering the electronic properties, when energies involved (in the device) remain close to the energy gap. The influence of the interface subO Si atoms is further analysed next.

#### V. ROLE OF INTERFACES

In order to assess the role of the subO ions on the electronic properties, we calculated the bandstructures of the FRM2/H/vacuum structure, Fig. 5(c), which contains *no* subO Si; the dangling bonds have been filled by hydrogen atoms and then structurally relaxed. Figure 9 summarizes the results. The band gap is still direct

but significantly lowered, from 0.81 eV in the FRM2 to 0.67 eV in the FRM2/H/vacuum structure. This value (0.67 eV) is 0.2 eV lower than that calculated by Agrawal and Agrawal<sup>21</sup> which involves no oxygen and no interface relaxation. Interface reconstruction (as discussed in section III and Fig. 3) thus has significant impact on the electronic properties. The bands in the plane orthogonal to the growth axis are quite different from FRM2; e.g., the valence band is lowered near the  $M$  and  $R$  points, becoming similar to the c-Si bandstructure. We thus conclude that the subO Si atoms have two effects: (i) increase the bandgap and (ii) produce dispersionless valence bands. The charge states in the subO are responsible for the increase in the bandgap, while the strongly increased valence-band offset leads to essentially dispersionless bands.

## VI. BLUESHIFT AND OPTICAL ENHANCEMENT

The matrix elements entering the calculations of the optical properties are often approximated as a constant in a given range of energies. However, such an approximation is inadequate for elucidating the enhanced luminescence in Si/SiO<sub>2</sub> SLs. This section deals with calculating the absorption coefficient within the Fermi Golden rule and interband-transition theory.

Since the Si-layer thickness  $L_{\text{Si}}$  is relevant to the energy-shift in SLs, this quantity needs first to be defined. This involves some uncertainty associated with the interface thicknesses  $L_{\text{subO}}$ .

The interface thickness  $L_{\text{subO}}$  was estimated to be  $\sim 1.60$  Å from our calculations of the subO Si region. This is the largest distance (projected onto the  $z$  axis) between any two subO Si atoms. Hence the upper-bound to  $L_{\text{Si}}$  are, 11.17 Å, 16.58 Å and 22.01 Å for the FRM1, FRM2 and FRM3 respectively, while the lower-bound thicknesses are simply  $L_{\text{Si}} - 2L_{\text{subO}}$ . We define the Si thickness in the SLs to include the interface subO Si atoms as well (corresponding to the upper bound). This choice is made since subO Si ( $\text{Si}^{+1}$ ,  $\text{Si}^{+2}$  or  $\text{Si}^{+3}$ ) atoms contribute to the electronic properties, as do bulk-Si atoms ( $\text{Si}^0$  atoms); for instance, we showed above [see e.g. Fig. 8(b)] that the bandstructures of the FRM2 SLs and the FRM2/O-H/vacuum systems overlap, and indicated where the effective barrier begins.

The band gaps of the FRM1, FRM2 and FRM3 (see the bandstructures in Fig. 7) are direct except for the FRM1 where the band gap is *nearly* direct with only 0.12 eV between the direct and indirect transitions. The values of the gap are 0.99 eV, 0.81 eV and 0.68 eV for the FRM1, FRM2 and FRM3, respectively. The direct transition at  $\Gamma$  for the FRM1 equals 1.11 eV. For the FRM2 and the FRM3, the band gaps are direct and located on the whole  $Z-\Gamma$  axis [see Fig. 7(b) and (c)]. Direct transitions can thus be achieved between the valence band and the conduction band, along the  $Z-\Gamma$  line of the BZ. We

thus obtain, under the LDA, a blue shift

$$0.68 \text{ eV} \longrightarrow 0.81 \text{ eV} \longrightarrow 0.99 \text{ eV}$$

with increased confinement

$$2.2 \text{ nm} \longrightarrow 1.7 \text{ nm} \longrightarrow 1.1 \text{ nm}.$$

However, these values for the energy gaps are much lower than the experimental ones. It is well known that DFT within the LDA underestimates the energy gaps of semiconductors and insulators. For c-Si, the DFT-LDA gap is approximately 0.6 eV less than the experimental value. For the  $\beta$ -cristobalite phase of SiO<sub>2</sub>, in the group  $I42d$ , the DFT-LDA energy gap is 5.8 eV while the experimental value is about 3 eV higher, i.e.,  $\sim 9$  eV. Approximate, but realistic, band gaps can be obtained by adding 0.6 eV overall:

$$\begin{array}{ccc} 1.28 \text{ eV} & \longrightarrow & 1.41 \text{ eV} & \longrightarrow & 1.59 \text{ eV}. \\ (2.2 \text{ nm}) & & (1.7 \text{ nm}) & & (1.1 \text{ nm}) \end{array}$$

These energy gaps correspond *exactly* to the lower bound of the experiments and lie in the visible spectrum.

The absorption of the three SL models and c-Si have been calculated both in the diamond-like BZ and in the SLs BZ. For c-Si in the diamond-like BZ, we used  $(20 \times 20 \times 20)$   $\mathbf{k}$  points,<sup>42</sup> while in the SLs BZ,  $(7 \times 7 \times 2)$   $\mathbf{k}$  points are used. Calculations using more  $\mathbf{k}$  points, viz.  $(8 \times 8 \times 3)$ , show that  $(7 \times 7 \times 2)$  is quite sufficient to recover the form of the absorption curve for all the SL models. The purpose of calculating the absorption of c-Si in two different BZ is to estimate errors, first due to zone folding effects (which cause round-off errors, leading to non-absolutely-null transitions at the onset)<sup>46</sup> and, second, to the tetrahedron method itself which needs large amounts of  $\mathbf{k}$  points. The broadening in the absorption curves has been fixed to 0.015 eV for all the absorption curves discussed below, as suggested by Fuggle.<sup>22</sup>

Figure 10 shows the absorption results. Panels (a) and (b) give an overall view of the absorption curves for the  $z$  axis in (a) and the  $x$ - $y$  plane in (b). Panels (c) and (d) show the absorption at the onset, for the  $z$  axis in (c) and the  $x$ - $y$  plane in (d). In all cases, we included the absorption of c-Si calculated in the diamond-like BZ, as well as the one in the SLs BZ. Direct comparison of the two c-Si absorption curves give an estimate of imprecisions due to zone foldings and intermediate number of  $\mathbf{k}$  point effects. It shows that the absorption is slightly underestimated in the SL calculations; e.g., in Fig. 10(c), the onset of absorption of c-Si in the SLs BZ take place at 2.0 eV while in the diamond-like BZ the onset happens at the correct value of 2.52 eV (which is for c-Si the LDA direct transition at  $\Gamma$ ). This numerical effect cannot be avoided and will arise, as well, in any Si/SiO<sub>2</sub> supercell. Hence, all comparison of the SLs absorption must be made with c-Si calculated in the equivalent SLs BZ, i.e., within equivalent  $\mathbf{k}$  space zone schemes.



Since the SLs are fabricated with the objective of changing the indirect gap to a direct gap, we now discuss the absorption threshold region. Comparison at the onset of absorption from Fig. 10(c) or (d) shows that all absorption curves have a lower energy threshold than *both* the c-Si absorption curves, and especially below the one calculated in equivalent SLs BZ having equal number of  $\mathbf{k}$  points. That is, *the SLs show absorption (and emission) in the spectral region above the indirect gap of c-Si and below the direct gap of c-Si*. This shows that the absorption in *all* confined Si/SiO<sub>2</sub> SL models is enhanced, compared to c-Si; the transitions are direct in SLs and have an active oscillator strength. For the folded c-Si energy bands, the lower bands above the Fermi level, and the corresponding oscillator strength, remain dark; in other words, the optical matrix elements of the SL BZ of c-Si are null up to  $\sim 2.0$  eV. This result clearly demonstrates the enhancement of the optical properties in confined Si structures. Furthermore, upon inspection of the absorption curves in the plane orthogonal to the growth axis [Fig. 10(d)], we note that the energy threshold of the absorption are all below c-Si: thus, the  $x$ - $y$  absorption of the FRMs take place approximately at their respective direct energy gaps, and then behave in a similar manner, as expected from the similarity of the SLs bandstructures, in this plane.

We examine, finally, the higher-energy region which corresponds to the usual direct transition (3 - 6 eV) in c-Si. Even here, Fig. 10(a) demonstrates a blueshift with increased confinement in the  $z$  axis. The overall absorption maxima for FRM1-FRM3 are at 5.28 eV, 4.83 eV, and 4.71 eV, with intensities of 136, 155 and 162 ( $\times 10^4/\text{cm}$ ) respectively. For c-Si in the SLs BZ (to ensure comparable precision in the calculations) the second peak, i.e., the maximum, take place at 4.70 eV (with absorption equal to  $231 \times 10^4/\text{cm}$ ), while the first peak is at 4.0 eV (and with absorption equal to  $229 \times 10^4/\text{cm}$ ). We emphasise that there is still a slight blueshift in the  $x$ - $y$  plane orthogonal to the growth axis, but less pronounced than in the growth axis.

## VII. CONCLUDING REMARKS

In this work, the structural, electronic and optical properties of Si/SiO<sub>2</sub> superlattices have been studied on the basis of structurally-relaxed models. These models, which contain no hydrogen atoms at the Si/SiO<sub>2</sub> interfaces, exhibit enhanced optical properties, as observed in experiment; this can be attributed to the presence of silicon dioxide barriers. In experiments performed under ultra-high vacuum conditions, the oxidation process would predominantly give rise to oxide bonds at the interfaces, but still, a few hydrogen atoms are expected to be present and fill some of the dangling bonds. Our calculations show that the oxide barrier is the main reason for the optical enhancement; extra hydrogen bonds at the interface would simply amplify the effect.

We have shown that suboxide Si atoms at the interfaces act as virtually impenetrable barriers. The active barrier thickness thus corresponds to the suboxide Si layer — only 1.6 Å in our models. The confined Si layer thus consists of bulk Si *and* suboxide Si atoms. Suboxide Si atoms at the interfaces modify the electronic properties in two manners: they (i) increase the energy gap and (ii) lead to dispersionless band structures, which increases the transition probabilities.

Further interface effects will be considered in future work. For instance, inclusion of other atomic species — such as nitrogen that would generate subnitric Si atoms at the Si/SiO<sub>2</sub> interface — are expected to modify the electronic properties, and hence enhance the optical characteristics.

*Acknowledgments* – It is a pleasure to thank Dr. Jurgen Furthmüller for help with the optical calculations in VASP. We gratefully acknowledge Dr. Z.-H. Lu for helpful discussions and suggestions. This work is supported by grants from the Natural Sciences and Engineering Research Council (NSERC) of Canada and the “Fonds pour la formation de chercheurs et l’aide à la recherche” (FCAR) of the Province of Québec. We are indebted to the “Réseau québécois de calcul de haute performance” (RQCHP) for generous allocations of computer resources.

- 
- \* Author to whom correspondence should be addressed:  
Email address: laurent.lewis@umontreal.ca
- <sup>1</sup> Z.H. Lu, D.J. Lockwood, and J.-M. Baribeau, *Nature* **378**, 258 (1995).
  - <sup>2</sup> Y. Kanemitsu and S. Okamoto, *Phys. Rev. B* **56**, R15561 (1997).
  - <sup>3</sup> S.V. Novikov, J. Sinkkonen, O. Kilpelä, and S. V. Gastev, *J. Vac. Sci. Technol. B* **15**, 1471 (1997).
  - <sup>4</sup> L. Khriachtchev, M. Räsänen, S. Novikov, O. Kilpelä, and J. Sinkkonen, *J. Appl. Phys.* **86**, 5601 (1999).
  - <sup>5</sup> V. Mulloni, R. Chierchia, C. Mazzeleni, G. Pucker, L. Pavesi, and P. Bellutti, *Philos. Mag. B* **80**, 705 (2000).
  - <sup>6</sup> Y. Kanemitsu, M. Liboshi, and T. Kushida, *Appl. Phys. Lett.* **76**, 2200 (2000).
  - <sup>7</sup> L.T. Canham, *Appl. Phys. Lett.* **57**, 1046 (1990).
  - <sup>8</sup> V. Lehman and U. Gösele, *Appl. Phys. Lett.* **58**, 856 (1991).
  - <sup>9</sup> L. Tsyberkov, K.L. Moore, D.G. Hall, and P.M. Fauchet, *Phys. Rev. B* **54**, R8361 (1996).
  - <sup>10</sup> S. Cheylan and R.G. Elliman, *Appl. Phys. Lett.* **78**, 1912 (2001).
  - <sup>11</sup> W.L. Ng, M.A. Lourenço, R.M. Gwilliam, S. Ledain, G. Shao, and K.P. Homewood, *Nature* **410**, 192 (2001).
  - <sup>12</sup> P. Schmuki, L.E. Erickson, and D.J. Lockwood, *Phys. Rev. Lett.* **80**, 4060 (1998).
  - <sup>13</sup> S. Schuppler, S.L. Friedman, M.A. Marcus, D.L. Adler, Y.-H. Xie, F.M. Ross, Y.J. Chabal, T.D. Harris, L.E. Brus, W.L. Brown, E.E. Chaban, P.F. Szajowski, S.B. Christman, and P.H. Citrin, *Phys. Rev. B* **52**, 4910 (1995); D.J. Lockwood, A. Wang, and B. Bryskiewicz, *Solid State Comm.* **89**, 587 (1994).
  - <sup>14</sup> Z.H. Lu (private communication).
  - <sup>15</sup> M. Zacharias, J. Bläsing, K. Hirschman, L. Tsyberkov, P.M. Fauchet, *J. Non-Crys. Solids* **266-269**, 640 (2000).
  - <sup>16</sup> B. Delley and E.F. Steigmeier, *Appl. Phys. Lett.* **67**, 2370 (1995).
  - <sup>17</sup> H. Kageshima and K. Shiraishi, in *Materials and Devices for Silicon-Based Optoelectronics*, edited by J.E. Cunningham, S. Coffa, A. Polman, and R. Soref, *Mater. Res. Soc. Symp. Proc. No. 486* (Material Research Society, Pittsburgh, 1998), pp.337.
  - <sup>18</sup> M.P.J. Pukkinen, T. Korhonen, K. Kokko, and I.J. Värynen, *Phys. Stat. Sol.* **214**, R17 (1999).
  - <sup>19</sup> E., Degoli, S. Ossicini, *Surf. Sci.* **470**, 32 (2000).
  - <sup>20</sup> P. Carrier, L.J. Lewis, and M.W.C. Dharma-wardana, *Phys. Rev. B* **64**, 195330-1 (2001).
  - <sup>21</sup> B.K. Agrawal and S. Agrawal, *Appl. Phys. Lett.* **77**, 3039 (2000).
  - <sup>22</sup> J.C. Fuggle, in *Unoccupied Electronic States*, edited by J.C. Fuggle and J.E. Inglesfield, *Topics in Applied Physics Vol. 69* (Springer-Verlag, Berlin, 1992).
  - <sup>23</sup> M.T. Sieger, D.A. Luh, T. Miller, and T.-C. Chiang, *Phys. Rev. Lett.* **77**, 2758 (1996); Z.H. Lu, M.J. Graham, D.T. Jiang, and K.H. Tan, *Appl. Phys. Lett.* **63**, 2941 (1993); F.J. Himpsel, F.R. McFeely, A. Taleb-Ibrahimi, J.A. Yarmoff, and G. Holliger, *Phys. Rev. B* **38**, 6084 (1988).
  - <sup>24</sup> D.J. Lockwood, Z.H. Lu, and J.-M. Baribeau, *Phys. Rev. Lett.* **76**, 539 (1996).
  - <sup>25</sup> A. Pasquarello, M.S. Hybertsen, and R. Car, *Appl. Surf. Sci.* **104/105** (1996) 317-322; A. Pasquarello, M.S. Hybertsen, and R. Car, *Appl. Phys. Lett.* **68**, 625 (1996).
  - <sup>26</sup> J.B. Neaton, D.A. Muller, and N.W. Ashcroft, *Phys. Rev. Lett.* **85**, 1298 (2000).
  - <sup>27</sup> Y. Tu and J. Tersoff, *Phys. Rev. Lett.* **84**, 4393 (2000).
  - <sup>28</sup> K.-O. Ng and D. Vanderbilt, *Phys. Rev. B* **59**, 10132 (1999).
  - <sup>29</sup> A. Stirling, A. Pasquarello, J.-C. Charlier, and R. Car, *Phys. Rev. Lett.* **85**, 2773 (2000).
  - <sup>30</sup> H. Kageshima and K. Shiraishi, *Phys. Rev. Lett.* **81**, 5936 (1998).
  - <sup>31</sup> F. Herman and I.P. Batra, in *The Physics of SiO<sub>2</sub> and its interfaces* edited by S.T. Pantelides (Pergamon, Oxford, 1978).
  - <sup>32</sup> N. Tit and M.W.C. Dharma-wardana, *Physics Letters A* **254**, 233 (1999).
  - <sup>33</sup> N. Tit and M.W.C. Dharma-wardana, *J. Appl. Phys.* **86**, 1 (1999).
  - <sup>34</sup> M. Tran, N. Tit, and M.W.C. Dharma-wardana, *Appl. Phys. Lett.* **75**, 4136 (1999).
  - <sup>35</sup> G. Kresse and J. Furthmüller, computer code **VASP 4.4** (Vienna University of Technology, Vienna, 1997) [Improved and updated Unix version of the original copyrighted VASP/VAMP code, which was published by G. Kresse and J. Furthmüller, *Comput. Mater. Sci.* **6**, 15 (1996)].
  - <sup>36</sup> G. Kresse and D. Joubert, *Phys. Rev. B* **59**, 1758 (1999).
  - <sup>37</sup> P. Hohenberg and W. Kohn, *Phys. Rev.* **136**, B864 (1964).
  - <sup>38</sup> W. Kohn and L.J. Sham, *Phys. Rev.* **140**, A1133 (1965).
  - <sup>39</sup> M.C. Payne, M.P. Teter, D.C. Allan, T.A. Arias, and J.D. Joannopoulos, *Rev. Mod. Phys.* **64**, 1045 (1992).
  - <sup>40</sup> P.E. Blöchl, *Phys. Rev. B* **50**, 17953 (1994).
  - <sup>41</sup> D.J. Singh, *Planewaves, pseudopotentials and the LAPW method*, (Kluwer Academic Publishers, Norwell, 1994).
  - <sup>42</sup> B. Adolph, J. Furthmüller, and F. Bechstedt, *Phys. Rev. B* **63**, 125108-1 (2001).
  - <sup>43</sup> P.Y. Yu and M. Cardona, *Fundamentals of Semiconductors* (Springer, New-York, 1996); G. Baym, *Lectures on Quantum mechanics*, (Addison-Wesley, Reading, 1993); L. Ley in *The Physics of Hydrogenated Amorphous Silicon II*, edited by J.D. Joannopoulos and G. Lucovsky, *Topics in Applied Physics*, Vol. **56** (Springer-Verlag, Berlin, 1984).
  - <sup>44</sup> P.E. Blöchl, *Phys. Rev. B* **49**, 16223 (1994).
  - <sup>45</sup> E.K. Chang, M. Rohlfing, and S.G. Louie, *Phys. Rev. Lett.* **85**, 2613 (2000); S. Albrecht, L. Reining, R. Del Sole, and G. Onida, *Phys. Rev. Lett.* **80**, 4510 (1998).
  - <sup>46</sup> J. Furthmüller (private communication).

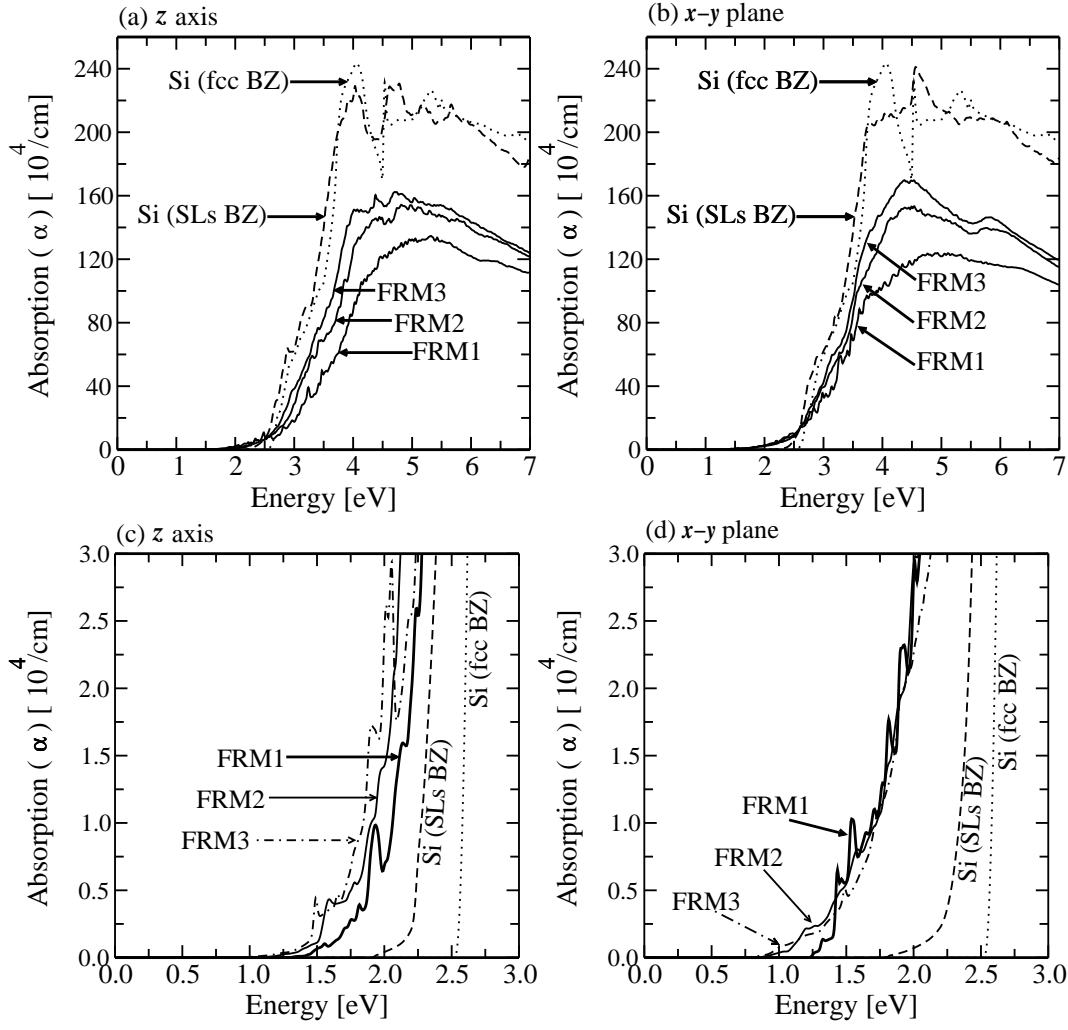


FIG. 10: Absorption coefficient of the SL models as compared to c-Si. (a) and (c) are the absorption in the growth axis; (b) and (d) are the absorption in the plane orthogonal to the growth axis.